Direct and Solvent-assisted Thione-thiol Tautomerism in 5-(Thiophen-2-yl)-1,3,4-oxadiazole-2(3H)-thione: Experimental and Molecular Modeling Study

ARTICLE *in* CHEMICAL PHYSICS · AUGUST 2014

Impact Factor: 1.65 · DOI: 10.1016/j.chemphys.2014.05.006

7 AUTHORS, INCLUDING:

Osman Dayan
Çanakkale Onsekiz Mart Üniversitesi
49 PUBLICATIONS **205** CITATIONS
SEE PROFILE

Necmi Dege
Ondokuz Mayıs Üniversitesi
63 PUBLICATIONS **195** CITATIONS
SEE PROFILE

Chemical Physics 439 (2014) 1–11

Contents lists available at ScienceDirect

Chemical Physics

journal homepage: www.elsevier.com/locate/chemphys

Direct and solvent-assisted thione–thiol tautomerism in 5-(thiophen-2-yl)-1,3,4-oxadiazole-2(3*H*)-thione: Experimental and molecular modeling study

N. Burcu Arslan [a], Namık Özdemir [b,*], Osman Dayan [c,*], Necmi Dege [b], Metin Koparır [d], Pelin Koparır [e], Halit Muğlu [f]

[a] Department of Computer Education and Instructional Technology, Faculty of Education, Giresun University, 28100 Giresun, Turkey
[b] Department of Physics, Faculty of Arts and Sciences, Ondokuz Mayıs University, 55139 Samsun, Turkey
[c] Laboratory of Inorganic Synthesis and Molecular Catalysis, Çanakkale Onsekiz Mart University, 17020 Çanakkale, Turkey
[d] Department of Chemistry, Faculty of Science, Fırat University, 23169 Elazığ, Turkey
[e] Department of Chemistry, Forensic Medicine Institute, 44000 Malatya, Turkey
[f] Department of Chemistry, Faculty of Arts and Sciences, Kastamonu University, 37200 Kastamonu, Turkey

ARTICLE INFO

Article history:
Received 2 February 2014
In final form 7 May 2014
Available online 21 May 2014

Keywords:
Crystal structure
IR and NMR spectroscopy
DFT
Thione–thiol tautomerism
Solvent effect

ABSTRACT

The compound has been synthesized and characterized by IR, NMR and X-ray diffraction. Quantum chemical calculations at B3LYP/6−311++G(d,p) level were performed to study the molecular and spectroscopic properties, conformational equilibrium, thione ↔ thiol tautomerism and intermolecular double proton transfer reaction of the compound. The obtained structural and spectroscopic results are well in agreement with the experimental data. The solvent effect on the proton transfer reaction was investigated in three solvents using the polarizable continuum model approximation and solvent-assisted mechanism. The *anti*-thione tautomer is the most stable isomer among the four possible structural forms both in the gas phase and in solution phase. A high tautomeric energy barrier is found for the tautomerism between the *anti* and *syn* forms of the compound, indicating a quite disfavored process. Although the presence of one methanol or water solvent molecule significantly lowers the energy barrier, it is not adequate for the reaction to occur.

1. Introduction

Because of their unique properties, the synthesis and applications of heterocyclics containing N, O, and S have attracted great interest among clinicians and investigators. Therefore, these compounds are widely investigated for their structural and molecular properties. Particularly, derivatives of 1,3,4-oxadiazole are known to have a broad spectrum of biological activities like antibacterial [1–4], fungitoxic [5,6], insecticidal [7], herbicidal [8], anticancer [9], anti-inflammatory [10], etc. On the other hand, the application of conducting polymer technologies of the compounds containing thiophene nucleus (another heterocyclic) was remarkable in addition to the biological activities of thiophene compounds [11,12].

In recent years, intra- or intermolecular proton transfer has been a topic of much interest because of its importance in many chemical and biological processes [13–16]. A large number of theoretical and experimental investigations have been carried out to enrich the information regarding the possible mechanisms of proton transfer, and tautomeric equilibria, and relevant properties associated with proton transfer [17–21]. In particular, the role played by the solvent in intra- or intermolecular proton transfer reactions is known to be crucial [22].

Mercapto-azoles can exist in two major tautomeric forms that exhibit different reactivities, as demonstrated for polymerization processes, metal complexation and substitution reactions [23–29]. In this respect, there are a growing interest in the scientific communities in experimental and theoretical investigation of thione–thiol tautomeric equilibrium of 1,3,4-oxadiazole-2-thione derivatives and their electronic structure [30–33].

In this work, the title 1,3,4-oxadiazole-2-thione compound has been newly synthesized by the ring-closure reaction of 2-thiophenecarboxylic acid hydrazide with carbon disulfide, and characterized with spectroscopic techniques such as FT-IR and NMR, and X-ray crystallography. The knowledge of the relative sta-

* Corresponding authors. Tel.: +90 362 3121919x5256; fax: +90 362 4576081 (N. Özdemir). Tel.: +90 286 2180018x1860; fax: +90 286 21805333 (O. Dayan).
E-mail addresses: namiko@omu.edu.tr (N. Özdemir), osmandayan@comu.edu.tr (O. Dayan).

http://dx.doi.org/10.1016/j.chemphys.2014.05.006
0301-0104/

bilities of tautomeric forms as well as of the transformation from one tautomeric form to another is important from the point of view of structural chemistry. Furthermore, knowing how the tautomerization energies change in various solvents gives an insight into the influence of solvents on molecular stability and reactivity. In the present study, we focus our attention on the thione–thiol tautomerization of the title 1,3,4-oxadiazole compound in both the gas phase and solution phase. In the first part of the latter case, bulk solvent effects (hereafter called direct solvent effect) are taken into account by using the polarized continuum model. In the second part, the proton transport catalyzed by a neutral solvent molecule is investigated. Chloroform, methanol and water are chosen as solvent. Intermolecular double proton transfer reaction (between hydrogen-bonded *anti*-thione and *anti*-thiol dimers) is also studied. All the calculations were performed at the DFT/B3LYP level of theory using the 6−311++G(d,p) basis function.

2. Materials and methods

2.1. General remarks

Starting chemicals were provided by Merck or Aldrich. Melting points were determined on a Thomas Hoover melting point apparatus and uncorrected, but checked by differential scanning calorimeter (DSC). KBr pellets on a Perkin-Elmer Spectrum one FT-IR spectrometer was used in order to record the FT-IR spectra of the compound in 4000–400 cm^{-1} region. The ^1H and ^{13}C spectra were taken on Bruker AC-400 NMR spectrometer operating at 400 MHz for ^1H and 100 MHz for ^{13}C NMR. The compound was dissolved in DMSO-d_6 and chemical shifts were referenced to TMS (^1H and ^{13}C NMR).

2.2. Synthesis

A mixture of 2-thiophenecarboxylic acid hydrazide (0.01 mol, 1.42 g), sodium hydroxide (0.01 mol, 0.4 g), carbon disulfide (0.02 mol, 1.2 ml) and absolute ethanol (100 ml) was heated under reflux for 12 h (Fig. 1). The excess solvent was removed by vacuum evaporation, and the residue was dissolved in water and acidified with acetic acid. The product was recrystallized from a mixture of ethanol and water (30:70) (yield: 65%; m.p.: 476–478 K).

2.3. X-ray crystallography

Reflection data were collected on a STOE IPDS II diffractometer at 296 K using graphite-monochromated Mo Kα radiation (λ = 0.71073 Å) and the ω-scan method. The structure was solved by direct methods using SHELXS-2013 [34] and refined with full-matrix least-squares calculations on F^2 using SHELXL-2013 [34] implemented in WinGX [35] program suit. All H atoms bonded to C atoms were positioned geometrically and refined as a riding model with C—H = 0.93 Å and $U_{iso}(H) = 1.2U_{eq}(C)$, while the H atom bonded to the N atom was located in a difference Fourier map and refined isotropically [N—H = 0.84(4) Å]. Data collection: X-AREA [36], cell refinement: X-AREA, data reduction: X-RED32 [36]. Details of the data collection conditions and the parameters of refinement process are given in Table 1. The general-purpose crystallographic tool PLATON [37] was used for the structure analysis.

CCDC 870045 contains supplementary crystallographic data (excluding structure factors) for the compound reported in this article. These data can be obtained free of charge *via* http://www.ccdc.cam.ac.uk/cgi-bin/catreq.cgi [or from the Cambridge Crystallographic Data Center (CCDC), 12 Union Road, Cambridge CB2 1EZ, UK; fax: +44(0)1223 336033; e-mail: data_request@ccdc.cam.ac.uk].

2.4. Computational methods

All calculations were carried out with the Gauss-View molecular visualization program [38] and Gaussian 03W program package [39]. The ground state geometries were fully optimized using the most popular B3LYP [40,41] method applying the 6−311++G(d,p) [42,43] basis sets without any symmetry restrictions and using the default convergence criteria. The geometry optimizations were followed by frequency calculations. So, the stationary structures are confirmed by ascertaining that all ground states have only real frequencies and all transition states have only one imaginary frequency. The ^1H and ^{13}C NMR chemical shifts were calculated within the gauge-independent atomic orbital (GIAO) approach [44,45] applying the same method and the basis set as used for geometry optimization. The Polarizable Continuum Model (PCM) [46–49] approximation was used to address the effect of bulk solvent at the same level.

3. Results and discussion

3.1. Description of the crystal structure

The title 1,3,4-oxadiazole-2-thione compound, a DIAMOND [50] view of which is shown in Fig. 2a, crystallizes in the monoclinic space group $P2_1/c$ with four molecules in the unit cell. The compound is composed of a thiophene ring bonded to the carbon atom

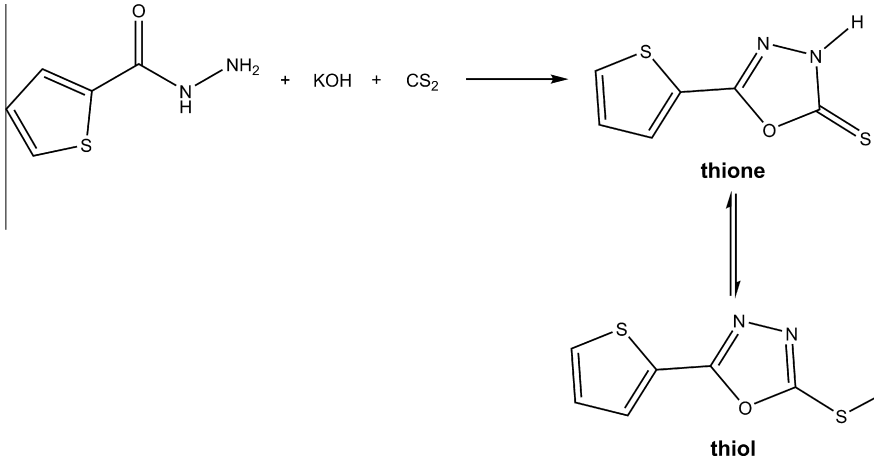

Fig. 1. Formation of the title compound.

Table 1
Crystal data and structure refinement parameters for the title compound.

CCDC deposition no.	955944
Color/shape	Colorless/plate
Chemical formula	$C_6H_4N_2OS_2$
Formula weight	184.23
Temperature (K)	296
Wavelength (Å)	0.71073 Mo Kα
Crystal system	Monoclinic
Space group	$P2_1/c$ (no. 14)
Unit cell parameters	
a, b, c (Å)	5.5206(3), 19.7032(8), 7.3197(4)
α, β, γ (°)	90, 104.436(4), 90
Volume (Å^3)	771.05(7)
Z	4
D_{calc} (g/cm^3)	1.587
μ (mm^{-1})	0.626
Absorption correction	Integration
T_{min}, T_{max}	0.693, 0.881
F_{000}	376
Crystal size (mm^3)	0.51 × 0.40 × 0.20
Diffractometer/measurement method	STOE IPDS II/ω scan
Index ranges	$-6 \leqslant h \leqslant 6$, $-24 \leqslant k \leqslant 24$, $-9 \leqslant l \leqslant 9$
θ range for data collection (°)	$2.07 \leqslant \theta \leqslant 26.58$
Reflections collected	13053
Independent/observed reflections	1603/1294
R_{int}	0.091
Refinement method	Full-matrix least-squares on F^2
Data/restraints/parameters	1603/0/104
Goodness-of-fit on F^2	1.024
Final R indices [$I > 2\sigma(I)$]	$R_1 = 0.0485$, $wR_2 = 0.1370$
R indices (all data)	$R_1 = 0.0592$, $wR_2 = 0.1433$
$\Delta\rho_{max}$, $\Delta\rho_{min}$ (e/Å^3)	0.287, −0.444

at the 5-position of 1,3,4-oxadiazole-2-thione ring, and exists in the *anti*-conformation. The molecular structure of the title compound is planar, the r.m.s. deviation of the non-H atoms being 0.0267 Å. The dihedral angle between the mean planes of the oxadiazole and thiophene rings is 2.173(13)°.

The C1—N1 bond length [1.323(3) Å], which is intermediate between standard single C—N (1.47 Å) and double C=N (1.28 Å) bonds, is significantly longer than the C2—N2 bond length [1.281(3) Å]. Besides, the C1—S1 bond length [1.649(3) Å] confirms the multiple nature of this bond. The N1—C1 and C1—S1 bonds are the most sensitive indicator of the type of tautomeric form. The C1—S1 bond has a double bond character for the thione tautomer, while this bond exhibits single bond character in the thiol tautomer. On the contrary, the N1—C1 bond is a double bond in the thiol tautomer, whereas it is a single bond in the thione tautomer. As a consequence, the thione form is favored over the thiol form in the title compound since the N1—C1 and C1—S1 bond lengths show single and double bond characters, respectively. All bond lengths and angles are within the expected ranges [51] and are similar to those of the related molecules [52–56].

In the molecular structure of the title compound, there are no intramolecular interactions. In the crystal structure, only one H-bonding interaction is observed with the H···A, D···A and D—H···A geometric parameters being 2.50(4) Å, 3.335(3) Å and 170(3)°, respectively. In this interaction, thioamide atom N1 in the molecule at (x, y, z) acts as hydrogen-bond donor, *via* atom H1, to thiocarbonyl atom S1 in the molecule at $(-x, -y, -z + 1)$, so generating by inversion a centrosymmetric dimer, centered at $(0, 0, 1/2)$ and characterized by an R_2^2 motif [57]. The dimers are linked to each other *via* two π–π stacking interactions in which the oxadiazole and thiophene rings of the molecule at (x, y, z) and $(x, -y + 1/2, z + 1/2)$ are mutually parallel with the corresponding ring-centroid separations being 3.613(6) and 3.743(5) Å, respectively. Propagation of these stacking interactions then links the hydrogen-bonded dimers into chains running parallel to the [0 0 1] direction (Fig. 3).

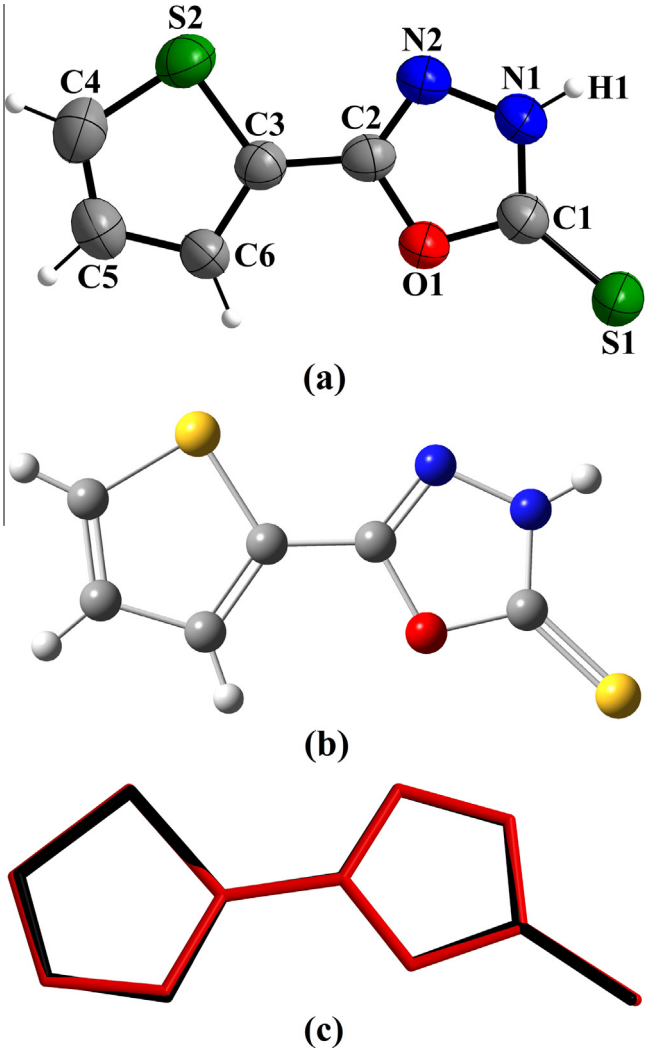

Fig. 2. (a) The molecular structure of the title compound showing the atom-numbering scheme. Displacement ellipsoids are drawn at the 50% probability level and H atoms are shown as small spheres of arbitrary radii. (b) The theoretical geometric structure of the title compound [B3LYP/6−311++G(d,p) level]. (c) Atom-by-atom superimposition of the structures calculated (red) over the X-ray structure (black) for the title compound. Hydrogen atoms omitted for clarity. (For interpretation of the references to color in this figure legend, the reader is referred to the web version of this article.)

3.2. Spectroscopic characterization

The FT-IR spectra of the compound are given in Fig. S1 (see Supplementary materials). The vibrational band assignments were made using the Gauss-View molecular visualization program, and a scale factor of 0.9668 [58] was used to correct the calculated vibrational frequencies. Some observed and calculated frequencies in the infrared spectra of the title compound and their probable assignments are given in Table S1 (see Supplementary materials). As can be seen from the table, an acceptable agreement exists between the experimental and theoretical vibrational frequencies.

Vibrations fall into the basic categories of stretching (ν) and bending. A stretching vibration involves a continuous change in the interatomic distance along the axis of the bond between two atoms. Bending vibrations are characterized by a change in the angle between two bonds and are of four types: scissoring (α), rocking (γ), wagging (ω) and twisting (δ). The first two bending modes are called "in-plane" and the second two are "out-of-plane". In scissoring, the two atoms joined to the central atom move

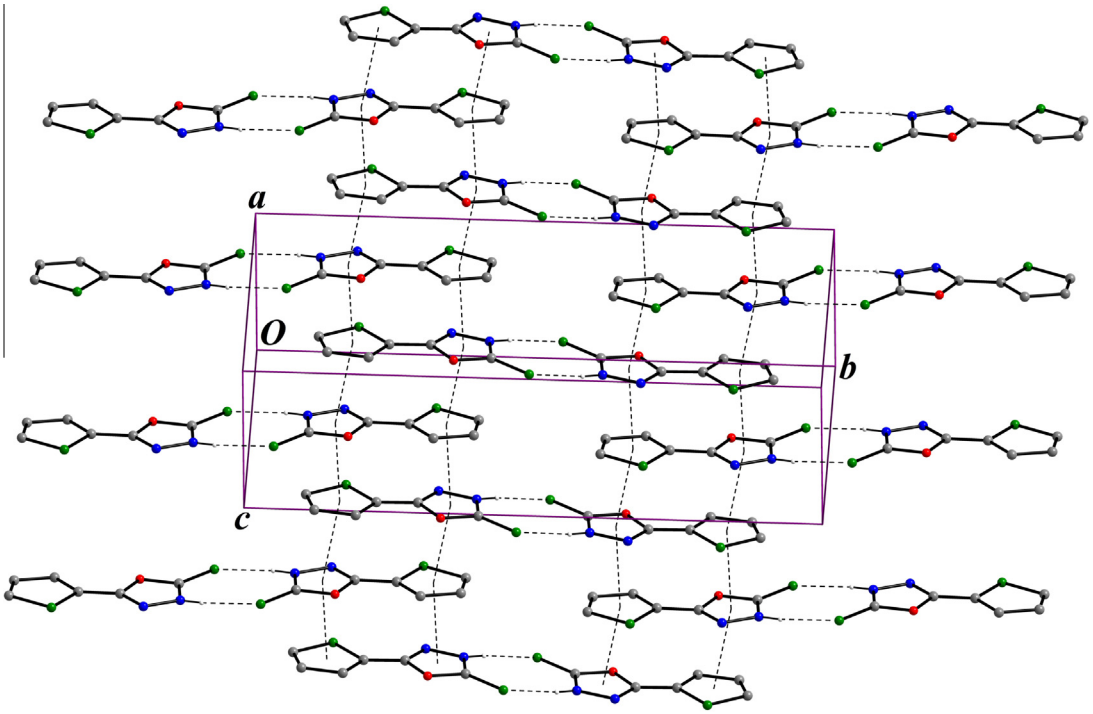

Fig. 3. Part of the crystal structure of the title molecule showing the formation of a π-stacked chain of centrosymmetric $R_2^2(8)$ dimers along [001]. For the sake of clarity, only H atoms involved in hydrogen bonding have been included.

towards and away from each other. In rocking, the structural unit swings back and forth in the plane of the molecule. In wagging, the structural unit swings back and forth out of plane of the molecule. In twisting, the structural unit rotates about the bond which joins it to the remainder of the molecule.

The high frequency region above 3000 cm^{-1} is the characteristic region for the ready identification of C—H, O—H and N—H stretching vibrations. It is stated that the N—H stretching frequency is usually observed in the region 3300–3500 cm^{-1} [59]. In the IR spectra of the compound, the absorption at 3128 cm^{-1} is assigned to the stretching vibrations of N—H bond that has been calculated at 3550 cm^{-1}. The difference between the experimental and theoretical values can be attributed to the N—H···S intermolecular H-bonding interaction. The N—H rocking and wagging modes recorded at 1423 and 458 $cm^{-1}$are in good agreement with theoretical results of 1449 and 460 cm^{-1}, respectively.

The C—H stretching, C—H in-plane bending and C—H out-of-plane bending vibrations appear in 2900–3150, 1100–1500 and 750–1000 cm^{-1} frequency ranges, respectively [60]. The C—H aromatic stretching modes are experimentally observed at 3102 and 3086 cm^{-1} and calculated at 3137 and 3103 cm^{-1}, respectively. Azomethine (C=N) bond stretching vibration of the compound is appeared at 1615 cm^{-1}, while it is computed at 1595 cm^{-1}. The bands at 1494 and 1374 cm^{-1} in the FT-IR spectra, which can be attributed to the ring C=C stretching vibrations, are calculated at 1498 and 1412 cm^{-1}, respectively. Stretching C=S vibration is seen in the experimental spectra at 1177 cm^{-1}, while the calculated value is predicted 49 cm^{-1} higher, at 1226 cm^{-1}. The other experimental and theoretical vibrational frequencies can be seen in Table S1.

Consequently, the characteristic vibration bands, such as N—H and C=S, belonging to only the thione tautomeric form of the compound as shown in Fig. 1 are observed in the FT-IR spectra, and these clearly indicate that the title compound has the thione form in the solid state.

The characterization of the compound was further enhanced by the use of ^1H and ^{13}C NMR spectroscopy. The ^1H and ^{13}C NMR spectra of the compound are shown in Figs. S2 and S3, respectively (see Supplementary materials). Theoretical chemical shift values are tabulated in Table S2 (see Supplementary materials) together with the experimental ones.

In the ^1H NMR spectra, thiophene backbone hydrogen's are observed as doublet of doublets at 7.20 ppm for *H5*, doublet at 7.71 ppm for *H6* and doublet at 7.85 ppm for *H4* that have been appeared at 7.4, 7.9 and 8.0 ppm in the theoretical spectra, respectively. The ^1H NMR spectra also exhibit a signal at 14.64 ppm as singlet due to oxadiazole N—H, while this signal is calculated at 9.0 ppm. The ^{13}C NMR spectra of the compound show C=S signals at 177.2 ppm and C=N signals at 157.1 ppm, which have been calculated at 181.1 and 166.2 ppm, respectively. The carbon peaks belonging to the thiophene ring are recorded at 123.7–131.9 ppm, while these signals are observed at 133.8–146.5 ppm theoretically.

3.3. Geometry, conformational equilibrium and thione–thiol tautomerism

Some selected geometrical parameters experimentally obtained and theoretically calculated both in the gas phase and in solution phase for the compound are listed in Table 2. As can be seen from the table, agreement between the experimental and theoretical geometric parameters is satisfactory. According to X-ray crystallographic study, the dihedral angle between the mean planes of the oxadiazole and thiophene rings is 2.173(13)°. This angle is calculated at 0.105° for the gas phase, while it is found to be 0.030° for all solution phase calculations.

The close structural relationship between the calculated and experimentally observed structures is best demonstrated with RMS overlay errors of 0.045 Å in the gas phase and 0.043 Å for all solvents (Fig. 2c). The differences are related to the fact that the theoretical calculations are based on the isolated molecules in the gas and solution phases, while the experimental results are based on the molecules in the crystal lattice.

The title compound can exist in two possible tautomeric forms; namely thione and thiol (see Fig. 1). Since the conformational flex-

Table 2
Experimental and optimized structural parameters of the *anti*-thione and *anti*-thiol tautomers, and transition state of the title compound.

Parameters	X-ray	Gas phase			Chloroform (ε = 4.90)			Methanol (ε = 32.63)			Water (ε = 78.39)		
		Thione	TS	Thiol	Thione	TS	Thiol	Thione	TS	Thiol	Thione	TS	Thiol
Bond lengths (Å)													
S1—C1	1.649(3)	1.640	1.707	1.752	1.652	1.712	1.750	1.657	1.713	1.749	1.658	1.714	1.749
S1—H1	–	–	–	1.349	–	–	1.348	–	–	1.348	–	–	1.348
O1—C1	1.359(3)	1.385	1.337	1.360	1.377	1.335	1.359	1.374	1.335	1.358	1.374	1.335	1.358
O1—C2	1.374(3)	1.371	1.400	1.376	1.373	1.399	1.374	1.373	1.398	1.372	1.373	1.398	1.372
N1—N2	1.379(3)	1.372	1.382	1.396	1.373	1.385	1.398	1.373	1.386	1.399	1.373	1.386	1.399
N1—C1	1.323(3)	1.356	1.314	1.292	1.347	1.311	1.294	1.344	1.310	1.295	1.344	1.310	1.295
N1—H1	0.84(4)	1.007	–	–	1.009	–	–	1.010	–	–	1.010	–	–
N2—C2	1.281(3)	1.293	1.297	1.295	1.295	1.299	1.297	1.295	1.300	1.297	1.295	1.300	1.297
S2—C3	1.710(2)	1.745	1.745	1.744	1.746	1.746	1.745	1.746	1.746	1.746	1.746	1.746	1.746
S2—C4	1.678(3)	1.726	1.729	1.729	1.728	1.729	1.729	1.728	1.729	1.729	1.728	1.729	1.729
C2—C3	1.426(4)	1.438	1.437	1.439	1.436	1.436	1.438	1.436	1.435	1.438	1.436	1.435	1.438
Bond angles (°)													
O1—C1—S1	123.70(19)	125.72	138.83	116.91	124.94	138.86	116.72	124.66	138.88	116.69	124.63	138.88	116.69
N1—C1—S1	131.3(2)	131.20	110.67	129.76	131.34	110.45	130.25	131.38	110.35	130.40	131.38	110.35	130.41
C1—S1—H1	–	–	–	92.66	–	–	93.26	–	–	93.44	–	–	93.46
O1—C1—N1	105.0(2)	103.08	110.50	113.33	103.72	110.69	113.03	103.96	110.77	112.91	103.99	110.77	112.90
O1—C2—N2	112.7(2)	113.04	112.69	111.92	112.64	112.56	111.73	112.50	112.52	111.66	112.49	112.55	111.66
O1—C2—C3	117.9(2)	118.66	117.81	118.72	118.80	117.88	118.74	118.87	117.92	118.80	118.88	117.93	118.80
N1—N2—C2	103.1(2)	103.26	104.25	106.91	103.42	104.26	106.90	103.48	104.26	106.89	103.49	104.25	106.89
N2—N1—C1	112.9(2)	113.70	109.59	105.85	113.38	109.43	105.91	113.26	109.37	105.92	113.25	109.36	105.92
N2—C2—C3	129.4(2)	128.31	129.50	129.36	128.56	129.57	129.53	128.63	129.56	129.54	128.63	129.56	129.54
C3—S2—C4	91.42(14)	90.86	90.90	90.95	90.87	90.91	90.98	90.88	90.91	91.00	90.88	90.91	91.00
C1—O1—C2	106.21(19)	106.93	102.98	101.98	106.85	103.07	102.43	106.79	103.09	102.61	106.79	103.10	102.63
N2—N1—H1	126.0(2)	120.80	–	–	120.61	–	–	120.56	–	–	120.56	–	–
C1—N1—H1	120.0(2)	125.50	–	–	126.01	–	–	126.18	–	–	126.19	–	–
Torsion angles (°)													
O1—C2—C3—S2	178.03(17)	−179.901	179.98	−179.98	−179.97	179.91	−179.99	−179.97	179.97	−179.99	−179.97	−180.00	−179.99
N2—C2—C3—S2	−0.6(4)	0.11	−0.02	0.02	0.03	−0.05	0.01	0.03	−0.03	0.01	0.03	0.01	0.01
O1—C2—C3—C6	−2.1(4)	0.10	−0.01	0.02	0.03	−0.11	0.01	0.03	−0.04	0.01	0.03	0.00	0.01
N2—C2—C3—C6	179.2(3)	−179.88	179.99	−179.98	−179.97	179.93	−179.99	−179.97	179.97	−179.99	−179.9	−180.00	−180.00

Note: ε = dielectric constant.

ibility over the C—C bond connecting the oxadiazole and thiophene rings allows the molecule to have different rotameric forms, a preliminary search of low energy structures was performed for both the thione and thiol tautomers using the B3LYP/6−311++G(d,p) computations as a one-dimensional scan by varying the φ(O1—C2—C3—S2) dihedral angle from −180° to 0° in steps of 5°. Molecular energy profiles with respect to rotations around the C2—C3 bond are presented in Fig. 4. According to the results, the title compound may exist in four structural forms, namely *anti*-thione, *syn*-thione, *anti*-thiol and *syn*-thiol.

The energy trend of the four relevant conformers was found as *anti*-thione < *syn*-thione < *anti*-thiol < *syn*-thiol. In particular, the *anti*-thione conformer was proved to be the most stable form. The relative energy of the *anti* and *syn* conformers was computed to be 3.43 kJ mol^{-1} for the thione tautomer, and 2.01 kJ mol^{-1} for the thiol tautomer. Calculated energy barriers for *anti* → *syn* isomerization were found to be 24.03 and 22.10 kJ mol^{-1} for the thione and thiol tautomers, respectively, while these barriers were calculated as 20.60 and 20.09 kJ mol^{-1} in the reverse direction.

Some selected structural parameters belonging to the *anti*-thione, *anti*-thiol and transition state (TS) geometries of the title compound optimized at the B3LYP/6−311++G(d,p) level are listed in Table 2, while the energies of the *anti*-thione and *anti*-thiol forms, energy differences and activation energies are given in Table 3. The obtained imaginary vibrational frequency of the transition state corresponding to the proton transfer is 1672i cm^{-1} for the gas phase, 1724i cm^{-1} for chloroform, 1746i cm^{-1} for methanol and 1748i cm^{-1} for water.

The thione and thiol tautomers could be converted to each other *via* an intramolecular proton transfer reaction. Due to the migration of a hydrogen atom from atom N1 to atom S1, some changes are observed in the structural parameters. On going from the thione to the thiol monomer, the N1—C1 bond length is reduced from 1.356 to 1.292 Å (from 1.347 to 1.294 Å for chloroform, from 1.344 to 1.295 Å for methanol and water), while the S1—C1 distance increases from 1.640 to 1.752 Å (from 1.652 to 1.750 Å for chloroform, from 1.657 to 1.749 Å for methanol and from 1.658 to 1.749 Å for water). This is consistent with the breaking of the S=C double bond and corresponding formation of an N=C double bond. As can be seen from Table 2, the N1—N2 distance increases, while the O1—C1 distance decreases in the proton transfer thione → TS → thiol. In addition, the O1—C1—S1, N1—C1—S1, O1—C2—N2, N2—N1—C1 and C1—O1—C2 angles contract as the O1—C1—N1, N1—N2—C2 and N2—C2—C3 angles expand.

The N1···H1 and S1···H1 distances for TS structure are found to be 1.355 and 1.760 Å in the gas phase, 1.358 and 1.756 Å in chloroform, 1.359 and 1.754 Å in methanol, and 1.359 and 1.754 Å in water, respectively. From a structural point of view, all results indicate that the TS structure resembles the structure of the thione tautomer rather than that of the thiol tautomer, since the transferred proton is closer to that observed for the thione than for the thiol form.

The energy profile of the single proton transfer process (thione → thiol tautomerism) is shown in Fig. 5. The tautomerization energy, as shown in Fig. 5, was calculated as the energy differences between the tautomers and the transition state. The energy differences between the two tautomers were calculated to be −45.90 kJ mol^{-1} in the gas phase, −48.78 kJ mol^{-1} in chloroform, −49.61 kJ mol^{-1} in methanol and −49.69 kJ mol^{-1} in water. Considering the ground state energy of the thione and thiol tautomers as well as the tautomerization energies in Table 3 show that the

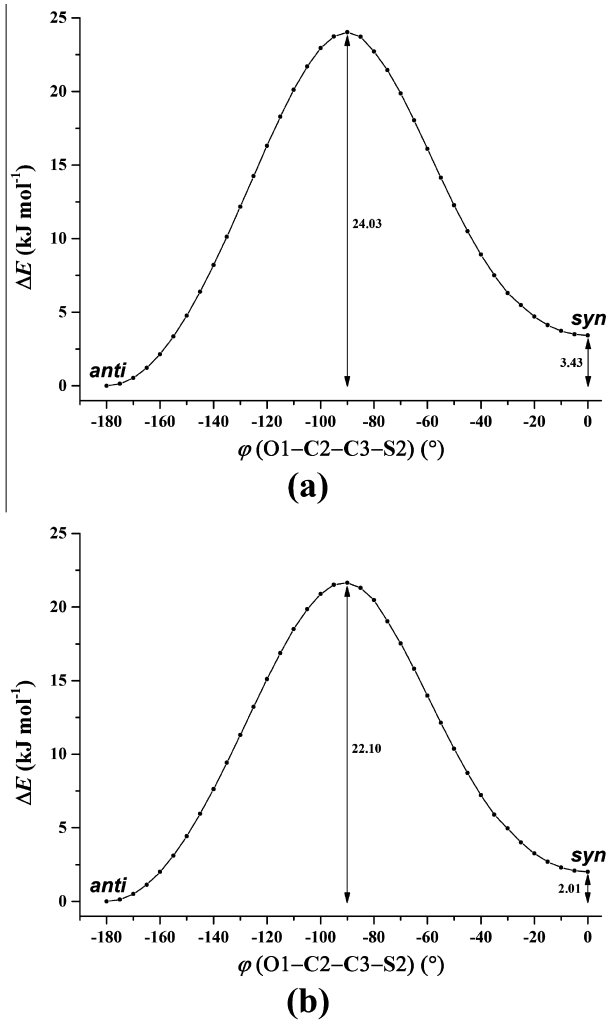

Fig. 4. The B3LYP/6−311++G(d,p) potential energy profiles for interconversion between two low energy forms of the thione (a) and thiol (b) tautomers of the title compound.

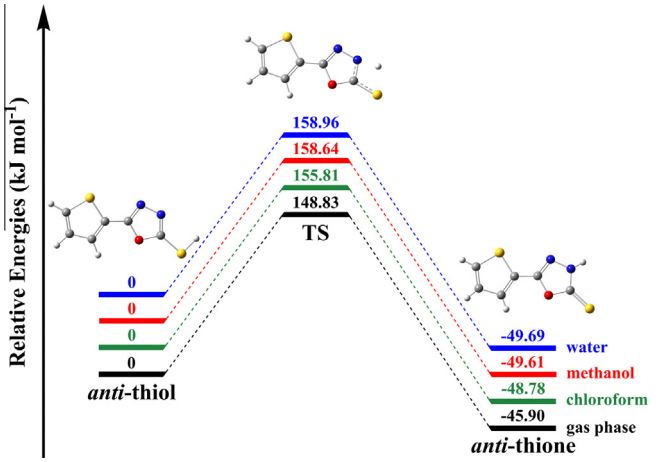

Fig. 5. Relative energy profile of the single proton transfer process (*anti*-thione/*anti*-thiol tautomerism) in the gas phase and various solvents.

thione form is more stable than the thiol case both in the gas phase and in solution phase.

The relative energies of the TS with respect to the thione tautomer were obtained as 194.73, 204.59, 208.25 and 208.65 kJ mol^{-1}, while the reverse reaction barriers were calculated as 148.83, 155.81, 158.64 and 158.96 kJ mol^{-1} in the gas phase, in chloroform, in methanol, and in water, respectively. These values show that considerable high energy is necessary for both the forward and the reverse proton transfer to occur. In both cases, the barrier height increases in going from the gas phase to water phase. High barrier energies in Table 3 suggest an unfavorable tautomerism both in the gas phase and in solution phase. It can be said that the stronger the dipole moment of the solvent, the higher the barrier to the proton transfer process.

The standard enthalpy and free energy changes for the single proton transfer are also listed in Table 3. As can be seen from the table, the large positive standard enthalpy and free energy changes for both the forward and the reverse proton transfer demonstrate that the thione → thiol and thiol → thione processes are highly endothermic reactions both in the gas phase and in solution phase. In conclusion, the single proton transfer is a quite disfavored process or not a spontaneous process.

Now we investigate the *anti*-thione → *anti*-thiol tautomerism in the presence of a single molecule of the same solvents. In this solvent-assisted case, the imaginary frequency is obtained as 469i cm^{-1} for chloroform, 692i cm^{-1} for methanol and 953i cm^{-1} for water. Geometries in Fig. 6 show some important geometrical changes as the tautomerism proceeds. Complexation with a single solvent molecule has a significant effect on the geometries of the thione and thiol units. As expected, the influence of the interaction with the solvent molecules on the bond distances and angles of thione and thiol tautomers shows themself mainly in the region of intermolecular hydrogen bondings.

The energies of the thione and thiol forms complexed with the solvent molecules, energy differences, activation energies, and standard enthalpy and free energy changes are given in Table 4. The energy differences between the two tautomers were found to be −41.53, −48.38 and −47.92 kJ mol^{-1} in going from chloroform to water, respectively. So, the thione form is more stable than thiol case.

The relative energies of the TS with respect to the thione tautomer were obtained as 220.16, 74.24 and 85.61 kJ mol^{-1}, while the reverse reaction barriers were calculated as 178.63, 25.86 and 37.69 kJ mol^{-1} in the presence of chloroform, methanol and water, respectively. Compared with the direct proton transfer process in the presence of the bulk solvent, it is seen that direct participation of solvent molecules reduces considerably the energy barrier, enthalpy and free energy changes for only methanol and water. However, large positive standard enthalpy and free energy changes

Table 3
Energies of the *anti*-thione and *anti*-thiol tautomers in hartree, and energy differences, activation energies and thermodynamic parameters in kJ mol^{-1}.

	Thione	Thiol	ΔE	E_a(f)	E_a(r)	ΔH_{298}(f)	ΔG_{298}(f)	$T\Delta S_{298}$(f)	ΔH_{298}(r)	ΔG_{298}(r)	$T\Delta S_{298}$(r)
Gas phase	−1212.28275949	−1212.26527900	−45.90	194.73	148.83	176.97	176.88	0.10	140.16	142.16	−2.00
Chloroform	−1212.29103380	−1212.27245281	−48.78	204.59	155.81	186.64	186.36	0.28	147.04	149.20	−2.17
Methanol	−1212.29419505	−1212.27529914	−49.61	208.25	158.64	190.26	189.90	0.36	149.83	151.95	−2.11
Water	−1212.29455187	−1212.27562416	−49.69	208.65	158.96	190.66	190.29	0.38	150.16	152.25	−2.10

$\Delta E = E_{thione} - E_{thiol}$, E_a(f) = forward activation energy, E_a(r) = reverse activation energy.

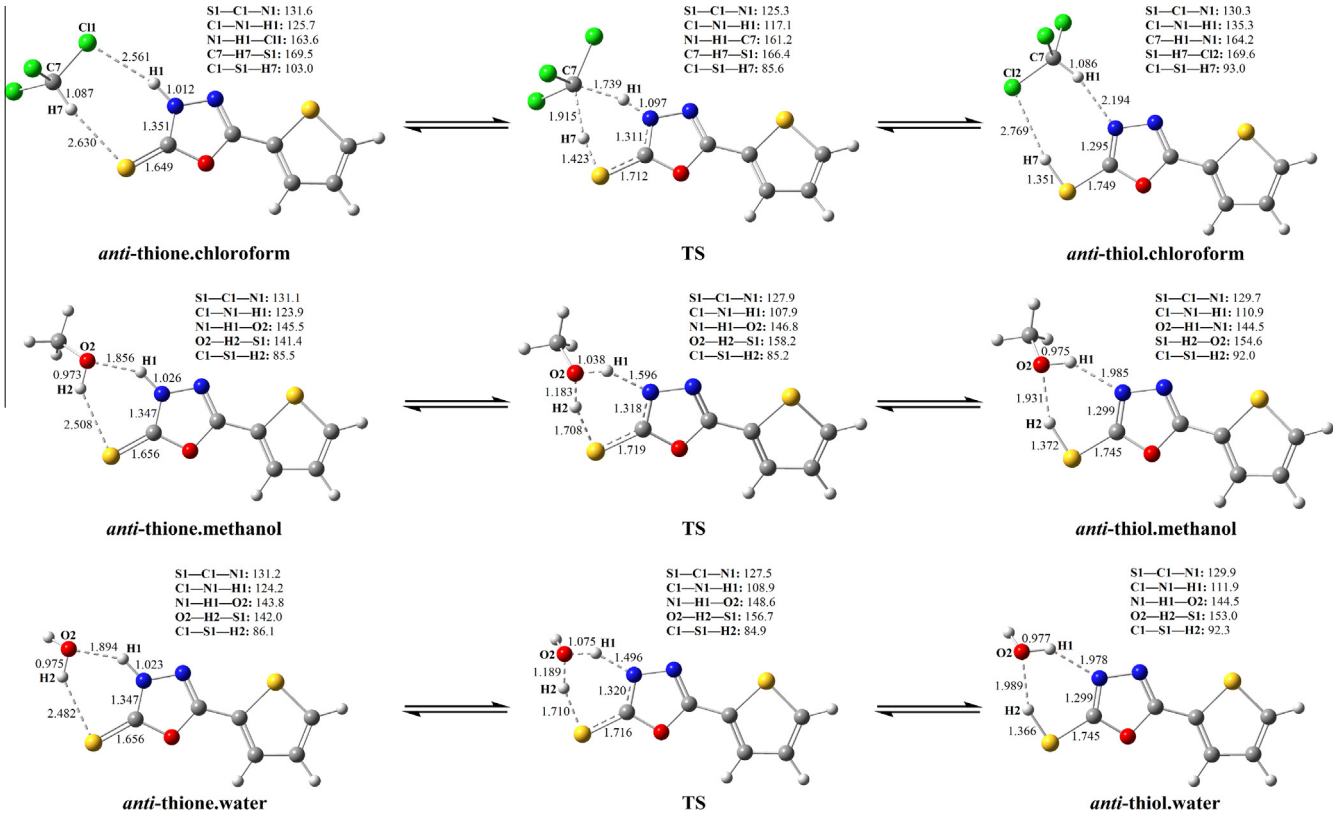

Fig. 6. Mechanism of solvent-assisted tautomerization between *anti*-thione and *anti*-thiol complexes by double proton transfer. Bond lengths are in angstroms and bond angles are in degree.

Table 4
Energies of the *anti*-thione and *anti*-thiol tautomers complexed with the solvent molecules in hartree, and energy differences, activation energies and thermodynamic parameters in kJ mol^{-1}.

	Thione	Thiol	ΔE	E_a(f)	E_a(r)	ΔH_{298}(f)	ΔG_{298}(f)	$T\Delta S_{298}$(f)	ΔH_{298}(r)	ΔG_{298}(r)	$T\Delta S_{298}$(r)
Chloroform	−2631.66948790	−2631.65367132	−41.53	220.16	178.63	198.25	208.77	−10.52	165.56	177.62	−12.06
Methanol	−1328.06406915	−1328.04564168	−48.38	74.24	25.86	56.92	65.82	−8.89	17.17	26.86	−9.69
Water	−1288.75726674	−1288.73901420	−47.92	85.61	37.69	66.39	75.42	−9.03	27.01	37.00	−9.99

$\Delta E = E_{\text{thione.solvent}} - E_{\text{thiol.solvent}}$, E_a(f) = forward activation energy, E_a(r) = reverse activation energy.

together with the tautomeric energy barrier reveal that high energy is also necessary for both the forward and the reverse proton transfer to occur in the presence of the solvent molecules, indicating a disfavored process or not a spontaneous process.

Some selected structural parameters belonging to the *syn*-thione, *syn*-thiol and transition state (TS) geometries of the title compound optimized at the same level are listed in Table 5, while the energies of the *syn*-thione and *syn*-thiol forms, energy differences and activation energies are given in Table 6. The obtained imaginary vibrational frequency of the transition state is 1673i cm^{-1} for the gas phase, 1724i cm^{-1} for chloroform, 1746i cm^{-1} for methanol and 1749i cm^{-1} for water.

On going from the thione to the thiol monomer, the N1—C1 bond length is reduced from 1.355 to 1.292 Å (from 1.347 to 1.294 Å for chloroform, from 1.344 to 1.294 Å for methanol and from 1.343 to 1.294 Å for water), while the S1—C1 distance increases from 1.640 to 1.752 Å (from 1.652 to 1.750 Å for chloroform, from 1.657 to 1.749 Å for methanol and from 1.658 to 1.749 Å for water). This is also consistent with the breaking of the S=C double bond and corresponding formation of an N=C double bond. As can be seen from Table 2, the N1—N2 distance increases, while the O1—C1 distance decreases in the proton transfer thione → TS → thiol. In addition, the O1—C1—S1, N1—C1—S1, O1—C2—N2, N2—N1—C1 and C1—O1—C2 angles contract while the O1—C1—N1, N1—N2—C2 and N2—C2—C3 angles expand. The N1···H1 and S1···H1 distances for TS structure are found to be 1.354 and 1.761 Å in the gas phase, 1.358 and 1.756 Å in chloroform, 1.359 and 1.754 Å in methanol and water, respectively. These results again show that the transition state resembles the thione than the thiol tautomer, with the transferred proton closer to that observed for the thione than for the thiol form.

The energy profile of the single proton transfer process is shown in Fig. 7. The energy differences between the two tautomers were calculated to be −44.48 kJ mol^{-1} in the gas phase, −48.07 kJ mol^{-1} in chloroform, −49.39 kJ mol^{-1} in methanol and −49.53 kJ mol^{-1} in water. Considering the ground state energy of the thione and thiol tautomers as well as the tautomerization energies in Table 6 show that the thione form is more stable than the thiol case both in the gas phase and in solution phase.

The relative energies of the TS with respect to the thione tautomer were obtained as 193.90, 204.23, 208.23 and 208.67 kJ mol^{-1}, while the reverse reaction barriers were calculated as 149.42, 156.16, 158.84 and 159.14 kJ mol^{-1} in the gas phase, in chloroform,

Table 5
Experimental and optimized structural parameters of the *syn*-thione and *syn*-thiol tautomers, and transition state of the title compound.

Parameters	Gas phase			Chloroform (ε = 4.90)			Methanol (ε = 32.63)			Water (ε = 78.39)		
	Thione	TS	Thiol	Thione	TS	Thiol	Thione	TS	Thiol	Thione	TS	Thiol
Bond lengths (Å)												
S1—C1	1.640	1.707	1.752	1.652	1.712	1.750	1.657	1.714	1.749	1.658	1.714	1.749
S1—H1	–	–	1.349	–	–	1.348	–	–	1.348	–	–	1.348
O1—C1	1.385	1.338	1.360	1.377	1.336	1.359	1.375	1.335	1.359	1.374	1.335	1.359
O1—C2	1.370	1.400	1.375	1.372	1.399	1.373	1.373	1.399	1.372	1.373	1.398	1.372
N1—N2	1.373	1.383	1.396	1.373	1.385	1.398	1.373	1.386	1.399	1.373	1.386	1.399
N1—C1	1.355	1.314	1.292	1.347	1.311	1.294	1.344	1.310	1.294	1.343	1.310	1.294
N1—H1	1.007	–	–	1.009	–	–	1.010	–	–	1.010	–	–
N2—C2	1.294	1.298	1.296	1.295	1.299	1.297	1.295	1.300	1.298	1.295	1.300	1.298
S2—C3	1.744	1.746	1.745	1.746	1.747	1.746	1.746	1.747	1.747	1.746	1.747	1.747
S2—C4	1.726	1.728	1.728	1.726	1.727	1.728	1.726	1.727	1.728	1.726	1.727	1.728
C2—C3	1.440	1.439	1.441	1.438	1.438	1.440	1.438	1.437	1.440	1.438	1.437	1.440
Bond angles (°)												
O1—C1—S1	125.80	138.96	116.94	125.02	138.98	116.71	124.70	139.01	116.65	124.66	139.00	116.64
N1—C1—S1	131.24	110.69	129.89	131.40	110.46	130.42	131.47	110.36	130.60	131.48	110.37	130.62
C1—S1—H1	–	–	92.67	–	–	93.31	–	–	93.52	–	–	93.54
O1—C1—N1	102.96	110.36	113.18	103.59	110.56	112.87	103.83	110.63	112.75	103.86	110.63	112.73
O1—C2—N2	113.04	112.68	111.92	112.62	112.52	111.73	112.47	112.47	111.65	112.45	112.47	111.65
O1—C2—C3	119.12	118.34	119.14	119.15	118.27	119.06	119.15	118.25	119.05	119.15	118.27	119.05
N1—N2—C2	103.17	104.18	106.80	103.35	104.20	106.80	103.42	104.20	106.80	103.42	104.20	106.80
N2—N1—C1	113.81	109.71	106.00	113.51	109.56	106.07	113.40	109.51	106.09	113.39	109.50	106.09
N2—C2—C3	127.84	128.98	128.93	128.23	129.22	129.21	128.38	129.28	129.30	128.40	129.26	129.31
C3—S2—C4	90.98	91.03	91.11	90.98	91.02	91.11	90.99	91.02	91.11	90.99	91.02	91.11
C1—O1—C2	107.02	103.08	102.10	106.94	103.16	102.54	106.89	103.19	102.72	106.89	103.20	102.74
N2—N1—H1	120.78	–	–	120.55	–	–	120.48	–	–	120.47	–	–
C1—N1—H1	125.41	–	–	125.94	–	–	126.13	–	–	126.15	–	–
Torsion angles (°)												
O1—C2—C3—S2	0.36	−0.06	0.30	0.37	0.03	0.37	0.37	−0.05	0.38	0.37	−0.07	0.38
N2—C2—C3—S2	−179.63	179.94	−179.73	−179.66	−179.98	−179.66	−179.65	179.96	−179.65	−179.65	179.92	−179.65
O1—C2—C3—C6	−179.66	179.93	−179.71	−179.65	−179.97	−179.64	−179.65	180.00	−179.63	−179.65	179.94	−179.63
N2—C2—C3—C6	0.35	−0.07	0.26	0.33	0.03	0.33	0.33	0.01	0.34	0.33	−0.07	0.35

Note: ε = dielectric constant.

Table 6
Energies of the *syn*-thione and *syn*-thiol tautomers in hartree, and energy differences, activation energies and thermodynamic parameters in kJ mol^{-1}.

	Thione	Thiol	ΔE	E_a(f)	E_a(r)	ΔH_{298}(f)	ΔG_{298}(f)	$T\Delta S_{298}$(f)	ΔH_{298}(r)	ΔG_{298}(r)	$T\Delta S_{298}$(r)
Gas phase	−1212.28145419	−1212.26451324	−44.48	193.90	149.42	176.14	175.92	0.23	140.72	142.55	−1.83
Chloroform	−1212.28984994	−1212.27153918	−48.07	204.23	156.16	186.14	185.35	0.79	147.32	148.98	−1.67
Methanol	−1212.29308664	−1212.27427640	−49.39	208.23	158.84	190.01	188.93	1.08	149.94	151.16	−1.22
Water	−1212.29345327	−1212.27458721	−49.53	208.67	159.14	190.46	159.26	1.20	150.24	151.30	−1.07

$\Delta E = E_{thione} - E_{thiol}$, E_a(f) = forward activation energy, E_a(r) = reverse activation energy.

in methanol, and in water, respectively. These values show that very high energy is necessary for both the forward and the reverse proton transfer to occur, and the barrier height increases in going from the gas phase to water phase. High barrier energies in Table 6 make the tautomerism unfavorable both in the gas phase and in solution phase. It is again seen that the stronger the dipole moment of the solvent, the higher the barrier to the proton transfer process.

The standard enthalpy and free energy changes for the single proton transfer are listed in Table 6. The large positive standard enthalpy and free energy changes obtained for both direction show that the thione → thiol and thiol → thione processes are highly endothermic reactions both in the gas phase and in solution phase. So, the single proton transfer is a quite disfavored process or not a spontaneous process.

In the solvent-assisted case, the imaginary frequency is obtained as 461i cm^{-1} for chloroform, 686i cm^{-1} for methanol and 951i cm^{-1} for water. Geometries in Fig. 8 show some important geometrical changes as the tautomerism proceeds. Complexation with a single solvent molecule has a significant effect on the geometries of the thione and thiol units. As expected, the influence of the interaction with the solvent molecules on the bond distances and angles of thione and thiol tautomers shows themself mainly in the region of intermolecular hydrogen bondings.

The energies of the thione and thiol forms complexed with the solvent molecules, energy differences, activation energies, and standard enthalpy and free energy changes are given in Table 7. The energy differences between the two tautomers were found to be −40.21, −47.44 and −46.96 kJ mol^{-1} in going from chloroform to water, respectively, approving that the thione form is more stable than thiol case.

The relative energies of the TS with respect to the thione tautomer were obtained as 218.88, 73.91 and 85.26 kJ mol^{-1}, while the reverse reaction barriers were calculated as 178.67, 26.47 and 38.30 kJ mol^{-1} in the presence of chloroform, methanol and water, respectively. Compared with the direct proton transfer process in the presence of the bulk solvent, it is seen that direct participation of solvent molecules reduces considerably the energy barrier, enthalpy and free energy changes for only methanol and water. However, large positive standard enthalpy and free energy changes together with the tautomeric energy barrier reveal that high energy is also necessary for both the forward and the reverse proton transfer to occur in the presence of the solvent molecules, indicating a disfavored process or not a spontaneous process.

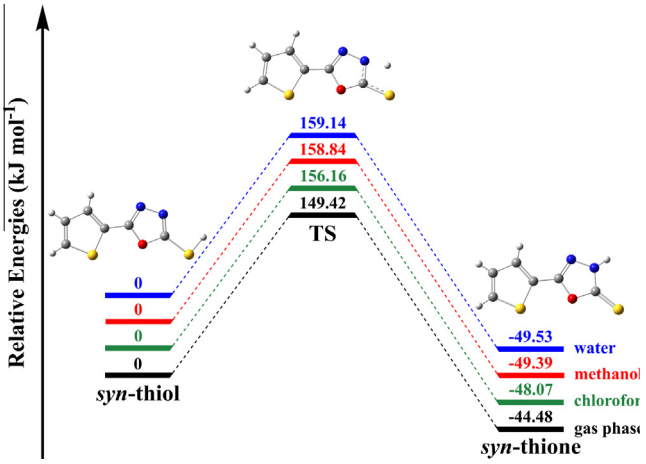

Fig. 7. Relative energy profile of the single proton transfer process (*syn*-thione/*syn*-thiol tautomerism) in the gas phase and various solvents.

3.4. Intermolecular double proton transfer reaction

In the crystal structure of the title compound, centrosymmetric dimers (*anti*-thione dimer) are formed *via* two N—H···S hydrogen bonds generating an R_2^2 ring. Since the energy barrier for the thione → thiol tautomerism of the compound is significantly reduced in the presence of methanol and water solvent molecules which form intermolecular hydrogen bonds with the tautomers, the proton transfer in this kind of system can be only an intermolecular process. To verify this possibility, the intermolecular double proton transfer reaction between the *anti*-thione and *anti*-thiol dimers has been investigated both in the gas phase and in solution phase at the same level of theory. Optimizations of the dimers were performed without symmetry constraints. Unfortunately, all attempts to optimize the transition state (TS) corresponding to the process *syn*-thione → *syn*-thiol dimers did not succeed.

Energies of the *anti*-thione and *anti*-thiol, energy differences, activation energies and thermodynamic parameters are given in Table 8. The calculated imaginary vibrational frequency of the transition state is 694i cm^{-1} for the gas phase, 898i cm^{-1} for chloroform, 905i cm^{-1} for methanol and 875i cm^{-1} for water.

The most remarkable changes in average bond lengths and angles in going from the monomer structures to the cyclic dimeric structures can be summarized as follows. In the thione dimer, the S1—C1 and N1—H1 bond lengths increase as a result of the N—H···S interactions, while the O1—C1 and N1—C1 distances decrease. In addition, the O1—C1—N1 and C1—N1—H1 angles become larger, while the O1—C1—S1 and N2—N1—C1 angles become smaller. In the thiol dimer, the S1—H1 and N1—C1 bond lengths increase as a result of the S—H···N interactions, while the S1—C1 distance decreases. Also, the O1—C1—S1, N2—N1—C1 and C1—O1—C2 angles expand as the O1—C1—N1 angle contracts. The average N1···H1 and S1···H1 distances for TS structure are found to be 1.473 and 1.516 Å in the gas phase, 1.556 and 1.492 Å in chloroform, 1.605 and 1.478 Å in methanol, and 1.580 and 1.483 Å in water, respectively.

The mechanism of the double proton transfer process between the *anti*-thione and *anti*-thiol dimers is given in Fig. 9. The energy differences between the two dimers were calculated to be −89.93, −96.03, −98.58 and −98.88 kJ mol^{-1} in going from gas phase to water phase, respectively. The ground state energy of the *anti*-thione and *anti*-thiol dimers as well as the energy differences between the two dimers and the transition state in Table 8 shows that the *anti*-thione dimer is more stable than *anti*-thiol dimer both in the gas phase and in solution phase.

The relative energies of the TS with respect to the thione dimer were obtained as 99.62, 98.54, 97.09 and 107.39 kJ mol^{-1} in the gas phase, in chloroform, in methanol, and in water, respectively. Similar to that of thione–thiol tautomerism, the barrier height

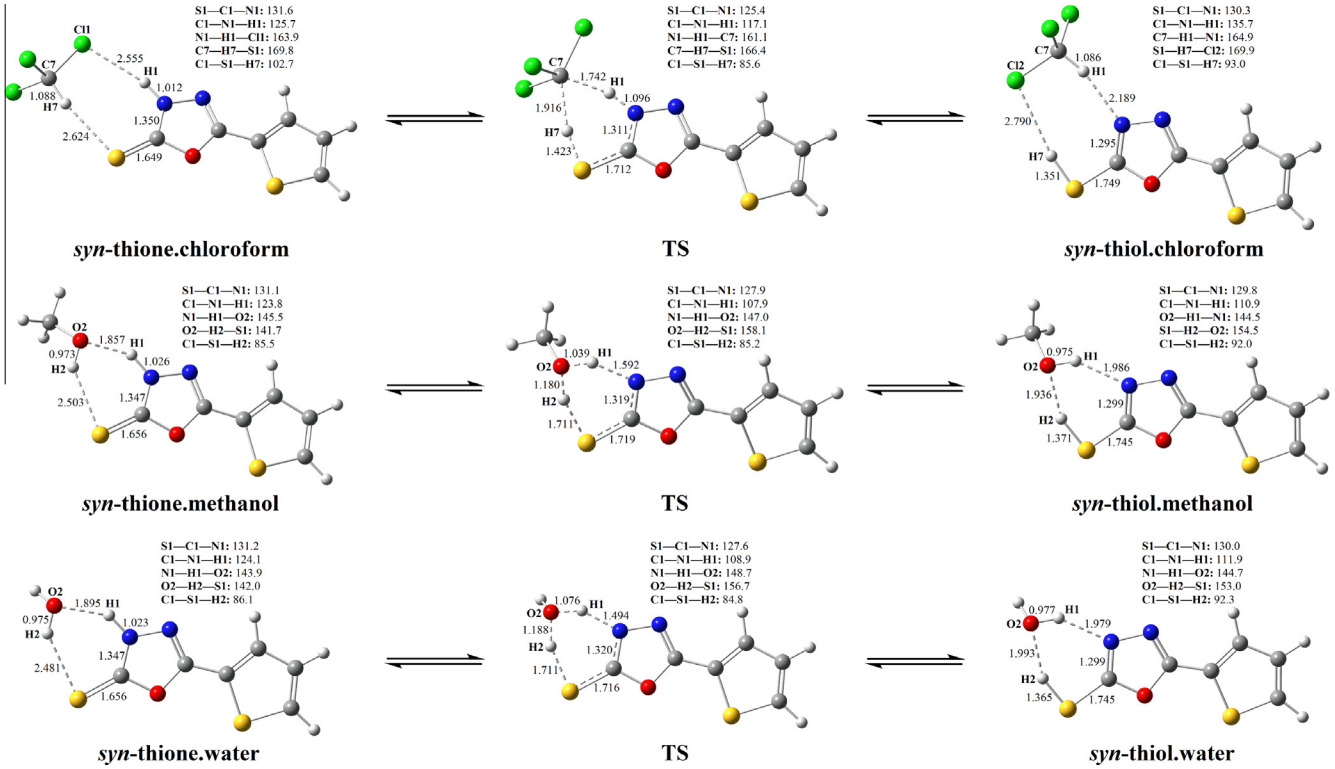

Fig. 8. Mechanism of solvent-assisted tautomerization between *syn*-thione and *syn*-thiol complexes by double proton transfer. Bond lengths are in angstroms and bond angles are in degree.

Table 7
Energies of the *syn*-thione and *syn*-thiol tautomers complexed with the solvent molecules in hartree, and energy differences, activation energies and thermodynamic parameters in kJ mol^{-1}.

	Thione	Thiol	ΔE	E_a(f)	E_a(r)	ΔH_{298}(f)	ΔG_{298}(f)	$T\Delta S_{298}$(f)	ΔH_{298}(r)	ΔG_{298}(r)	$T\Delta S_{298}$(r)
Chloroform	−2631.66822245	−2631.65290820	−40.21	218.88	178.67	197.09	207.20	−10.12	165.71	178.07	−12.36
Methanol	−1328.06281032	−1328.04474322	−47.44	73.91	26.47	56.57	65.15	−8.59	17.78	27.94	−10.16
Water	−1288.75603444	−1288.73814720	−46.96	85.26	38.30	65.94	74.67	−8.74	27.52	37.34	−9.82

$\Delta E = E_{\text{thione.solvent}} - E_{\text{thiol.solvent}}$, E_a(f) = forward activation energy, E_a(r) = reverse activation energy.

Table 8
Energies of the *anti*-thione and *anti*-thiol dimers in hartree, and energy differences, activation energies and thermodynamic parameters in kJ mol^{-1}.

	Anti-thione dimer	*Anti*-thiol dimer	ΔE	E_a(f)	E_a(r)	ΔH_{298}(f)	ΔG_{298}(f)	$T\Delta S_{298}$(f)	ΔH_{298}(r)	ΔG_{298}(r)	$T\Delta S_{298}$(r)
Gas phase	−2424.58424747	−2424.54999484	−89.93	99.62	9.69	68.52	69.27	−0.75	−3.40	−0.54	−2.86
Chloroform	−2424.59442002	−2424.55784371	−96.03	98.54	2.51	69.62	72.42	−2.80	−8.36	−2.65	−5.71
Methanol	−2424.59854512	−2424.56099657	−98.58	97.09	−1.49	68.65	72.11	−3.45	−11.82	−4.67	−7.15
Water	−2424.59902153	−2424.56135881	−98.88	107.39	8.50	79.19	79.62	−0.43	−1.56	2.70	−4.26

$\Delta E = E_{\textit{anti}\text{-thione dimer}} - E_{\textit{anti}\text{-thiol dimer}}$, E_a(f) = forward activation energy, E_a(r) = reverse activation energy.

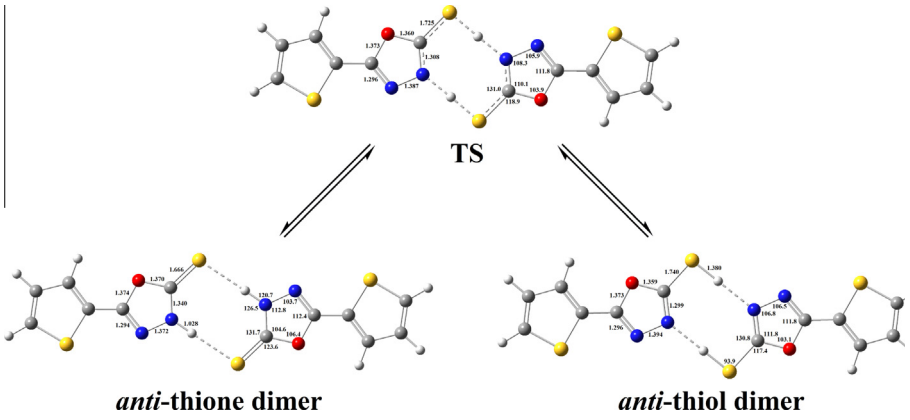

Fig. 9. Mechanism of double proton transfer process between *anti*-thione and *anti*-thiol dimers and corresponding transition structure (TS). Bond lengths are in angstroms and bond angles are in degree.

increases on going from the gas phase to water phase. It is seen that the stronger the dipole moment of the solvent, the higher the barrier to the proton transfer process. However, the reverse reaction has a low energy barrier with values of 9.69, 2.51 and 8.50 kJ mol^{-1} in the gas phase, in chloroform, and in water, respectively. Interestingly, the energy of TS is found to be smaller than that of the *anti*-thiol dimer in methanol, indicating no barrier. As a result, the reverse reaction is much easier than the forward proton transfer.

According to the standard enthalpy and free energy changes for the double proton transfer, the forward double proton transfer is found to be endothermic with large positive standard enthalpy and free energy changes both in the gas phase and in solution phase. The values of the standard enthalpies for the reverse reaction show that all the proton transfers are enthalpically favored (exothermic). However, the double proton transfer reaction in water needs larger entropy change rather than energy change to occur ($|T\Delta S_{298}| > |\Delta H_{298}|$). Therefore, this reaction is thermodynamically disfavored ($\Delta G_{298} > 0$).

4. Conclusions

In this paper, we have presented the results of experimental and theoretical investigations of the structural parameters, spectroscopic features, conformational equilibrium, thione ↔ thiol tautomerism and intermolecular double proton transfer reaction of the title 1,3,4-oxadiazole-2-thione compound. The direct solvent effect on the structure and single proton transfer reaction was studied in three kinds of solvents (chloroform, methanol and water) using Polarizable Continuum Model (PCM) method. In addition, the thione ↔ thiol tautomerism was also investigated in the presence of the same solvent molecules. The results of our studies can be summarized as follows:

1. In the solid state, the molecules exist in the thione form. The structural parameters of the title molecule calculated in the gas phase and in solvents are in very good correspondence with X-ray experimental data with RMS overlay errors of 0.045 and 0.043 Å for the gas phase and all solvents, respectively.
2. The main vibration bands as well as ^{1}H and ^{13}C NMR chemical shift values approve the thione form of the title compound spectroscopically.
3. In consonance with the theoretically predicted relative energies of the four conformers, *anti*-thione conformer is found to be the most stable one (*anti*-thione < *syn*-thione < *anti*-thiol < *syn*-thiol). Although the energy difference between the *anti* and *syn* conformers is small (*ca.* 2–3.5 kJ mol^{-1}), barrier energy for *anti* ↔ *syn* conformational interconversion is high (*ca.* 20–24 kJ mol^{-1}).
4. The predicted energy difference between *anti*-thione and *anti*-thiol tautomers is within the range *ca.* 46–50 kJ mol^{-1}, while the activation energy is within the range *ca.* 195–209 kJ mol^{-1}

for *anti*-thione → *anti*-thiol reaction, and within the range *ca.* 149–159 kJ mol^{-1} for *anti*-thiol → *anti*-thione reaction. Similarly, the energy difference between *syn*-thione and *syn*-thiol tautomers is within the range *ca.* 44.5–49.5 kJ mol^{-1}, while the activation energy is within the range *ca.* 194–209 kJ mol^{-1} for *syn*-thione → *syn*-thiol reaction, and within the range *ca.* 149–159 kJ mol^{-1} for *syn*-thiol → *syn*-thione reaction. In both cases, the barrier height for both the forward and the reverse single proton transfer reaction increases upon shifting from the gas phase to water phase. Thus, the tautomerization is not occurred from the thermodynamic and kinetic points of view both in the gas phase and in solution phase. These findings are also confirmed by large positive standard enthalpy and free energy changes.

5. When the participation of a single molecule of the same solvents in the proton-transfer reaction is taken into account, it is seen that the barrier height is reduced significantly only in the presence of methanol or water. Although the obtained values still make the tautomerization unfavorable, it is seen that the inclusion of more molecules of solvent as well as the effect of the bulk will probably reduce more these barriers.
6. When the dimerization of the *anti*-thione and *anti*-thiol tautomers is investigated, the *anti*-thione dimer is found to be more stable than *anti*-thiol dimer both in the gas phase and in solution phase, the energy differences being within the range *ca.* 90–99 kJ mol^{-1}. For the *anti*-thione dimer → *anti*-thiol dimer double proton transfer process, the barrier height is within the range *ca.* 100–107 kJ mol^{-1} indicating an unfavored process with large positive standard enthalpy and free energy changes. However, low energy barrier is found for the reverse reaction, within the range *ca.* 2.5–10 kJ mol^{-1}. Also, the transfer process in methanol phase can be assumed to be barrierless since the energy of TS is found between the two dimers.

Acknowledgment

We acknowledge the Faculty of Arts and Sciences, Ondokuz Mayıs University, Turkey, for the use of the STOE IPDS II diffractometer (purchased under Grant No. F-279 of the University Research Fund). We would also like to thank the reviewers for their helpful comments and suggestions to improve the manuscript.

Appendix A. Supplementary data

Supplementary data associated with this article can be found, in the online version, at http://dx.doi.org/10.1016/j.chemphys.2014.05.006.

References

[1] M.G. Mamolo, D. Zampieri, L. Vio, M. Fermeglia, M. Ferrone, S. Pricl, G. Scialino, E. Banfi, Bioorg. Med. Chem. 13 (2005) 3797.
[2] Y.A. Al-Soud, N.A. Al-Masoudi, J. Braz. Chem. Soc. 14 (2003) 790.
[3] S. Jain, N. Jain, P. Mishra, Indian J. Heterocycl. Chem. 14 (2005) 359.
[4] A.H. El-Masry, H.H. Fahmy, S.H.A. Abdelwahed, Molecules 5 (2000) 1429.
[5] X.J. Zou, L.H. Lai, G.Y. Jin, Z.X. Zhang, J. Agric. Food Chem. 50 (2002) 3757.
[6] I.A. Shehata, Saudi Pharm. J. 11 (2003) 87.
[7] S. Holla, C.S. Prasanna, B. Poojary, K.S. Rao, K. Shridhara, U.G. Bhat, Indian J. Chem. 43 (2004) 864.
[8] M.A.E. Shaban, A.Z. Nasr, S.M. El-Badry, J. Islamic Acad. Sci. 4 (1991) 184.
[9] A.S. Aboraia, H.M. Abdel-Rahman, N.M. Mahfouz, M.A. El-Gendy, Bioorg. Med. Chem. 14 (2006) 1236.
[10] M.M. Burbuliene, V. Jakubkiene, G. Mekuskiene, E. Udrenaite, R. Smicius, P. Vainilavicius, Il Farmaco 59 (2004) 767.
[11] J. Roncali, Chem. Rev. 92 (1992) 711.
[12] R. Mishra, K.K. Jha, S. Kumar, I. Tomer, Der Pharma Chemica 3 (2011) 38.
[13] J.M. Mayer, Acc. Chem. Res. 44 (2011) 36.
[14] C.M. Maupin, N. Castillo, S. Taraphder, C. Tu, R. McKenna, D.N. Silverman, G.A. Voth, J. Am. Chem. Soc. 133 (2011) 6223.
[15] M.-T. Zhang, T. Irebo, O. Johansson, L. Hammarström, J. Am. Chem. Soc. 133 (2011) 13224.
[16] D.R. Weinberg, C.J. Gagliardi, J.F. Hull, C.F. Murphy, C.A. Kent, B.C. Westlake, A. Paul, D.H. Ess, D.G. McCafferty, T.J. Meyer, Chem. Rev. 112 (2012) 4016.
[17] A.L. Sobolewski, W. Domcke, Chem. Phys. 294 (2003) 73.
[18] T. Schultz, E. Samoylova, W. Radloff, I.V. Hertel, A.L. Sobolewski, W. Domcke, Science 306 (2004) 1765.
[19] A. Bach, C. Tanner, C. Manca, H.-M. Frey, S. Leutwyler, J. Chem. Phys. 119 (2003) 5933.
[20] M. Meuwly, A. Bach, S. Leutwyler, J. Am. Chem. Soc. 123 (2001) 11446.
[21] R. Casadesús, M. Moreno, J.M. Lluch, Chem. Phys. 290 (2003) 319.
[22] M.C.P. Lima, K. Coutinho, S. Canuto, W.R. Rocha, J. Phys. Chem. A 110 (2006) 7253.
[23] A. Siwek, M. Wujec, I. Wawrzycka-Gorczyca, M. Dobosz, P. Paneth, Heteroat. Chem. 19 (2008) 337.
[24] B.S. Holla, M.K. Shivanda, P.M. Akberali, S. Baliga, S. Safeer, Il Farmaco 51 (1996) 785.
[25] E. Shouji, D.A. Buttry, J. Phys. Chem. B 102 (1998) 1444.
[26] A.R. Katritzky, Z. Wang, R.J. Offerman, J. Heterocycl. Chem. 27 (1990) 139.
[27] A.R. Katritzky, J. Borowiecka, W.Q. Fan, L.H. Brannigan, J. Heterocycl. Chem. 28 (1991) 1139.
[28] E.S. Raper, Coord. Chem. Rev. 153 (1996) 199.
[29] E.S. Raper, Coord. Chem. Rev. 165 (1997) 475.
[30] M. Koparır, A. Çetin, A. Cansız, Molecules 10 (2005) 475.
[31] D.D. Charistos, G.V. Vagenas, L.C. Tzavellas, C.A. Tsoleridis, N.A. Rodios, J. Heterocycl. Chem. 31 (1994) 1593.
[32] C.A. Tsoleridis, D.A. Charistos, G.V. Vagenas, J. Heterocycl. Chem. 34 (1997) 1715.
[33] F. Aydoğan, Z. Turgut, N. Öcal, S.S. Erdem, Turk. J. Chem. 26 (2002) 159.
[34] G.M. Sheldrick, Acta Crystallogr., Sect. A 64 (2008) 112.
[35] L.J. Farrugia, J. Appl. Crystallogr. 45 (2012) 849.
[36] Stoe, Cie, X-AREA Version 1.18 and X-RED32 Version 1.04, Stoe & Cie, Darmstadt, Germany, 2002.
[37] A.L. Spek, Acta Crystallogr. D65 (2009) 148.
[38] R. Dennington II, T. Keith, J. Millam, Gauss View, Version 4.1.2, Semichem Inc., Shawnee Mission, KS, 2007.
[39] M.J. Frisch, G.W. Trucks, H.B. Schlegel, G.E. Scuseria, M.A. Robb, J.R. Cheeseman, J.A. Montgomery Jr., T. Vreven, K.N. Kudin, J.C. Burant, J.M. Millam, S.S. Iyengar, J. Tomasi, V. Barone, B. Mennucci, M. Cossi, G. Scalmani, N. Rega, G.A. Petersson, H. Nakatsuji, M. Hada, M. Ehara, K. Toyota, R. Fukuda, J. Hasegawa, M. Ishida, T. Nakajima, Y. Honda, O. Kitao, H. Nakai, M. Klene, X. Li, J.E. Knox, H.P. Hratchian, J.B. Cross, V. Bakken, C. Adamo, J. Jaramillo, R. Gomperts, R.E. Stratmann, O. Yazyev, A.J. Austin, R. Cammi, C. Pomelli, J.W. Ochterski, P.Y. Ayala, K. Morokuma, G.A. Voth, P. Salvador, J.J. Dannenberg, V.G. Zakrzewski, S. Dapprich, A.D. Daniels, M.C. Strain, O. Farkas, D.K. Malick, A.D. Rabuck, K. Raghavachari, J.B. Foresman, J.V. Ortiz, Q. Cui, A.G. Baboul, S. Clifford, J. Cioslowski, B.B. Stefanov, G. Liu, A. Liashenko, P. Piskorz, I. Komaromi, R.L. Martin, D.J. Fox, T. Keith, M.A. Al-Laham, C.Y. Peng, A. Nanayakkara, M. Challacombe, P.M.W. Gill, B. Johnson, W. Chen, M.W. Wong, C. Gonzalez, J.A. Pople, Gaussian 03, Revision E.01, Gaussian Inc., Wallingford, CT, 2004.
[40] A.D. Becke, J. Chem. Phys. 98 (1993) 5648.
[41] C. Lee, W. Yang, R.G. Parr, Phys. Rev. B 37 (1988) 785.
[42] R. Krishnan, J.S. Binkley, R. Seeger, J.A. Pople, J. Chem. Phys. 72 (1980) 650.
[43] M.J. Frisch, J.A. Pople, J.S. Binkley, J. Chem. Phys. 80 (1984) 3265.
[44] R. Ditchfield, J. Chem. Phys. 56 (1972) 5688.
[45] K. Wolinski, J.F. Hinton, P. Pulay, J. Am. Chem. Soc. 112 (1990) 8251.
[46] S. Miertuš, E. Scrocco, J. Tomasi, Chem. Phys. 55 (1981) 117.
[47] V. Barone, M. Cossi, J. Phys. Chem. A 102 (1998) 1995.
[48] M. Cossi, N. Rega, G. Scalmani, V. Barone, J. Comput. Chem. 24 (2003) 669.
[49] J. Tomasi, B. Mennucci, R. Cammi, Chem. Rev. 105 (2005) 2999.
[50] K. Brandenburg, DIAMOND Demonstration Version 3.2.f, Crystal Impact GbR, Bonn, Germany, 2006.
[51] F.H. Allen, O. Kennard, D.G. Watson, L. Brammer, A.G. Orpen, R. Taylor, J. Chem. Soc., Perkin Trans. 2 (1987) S1.
[52] Y.-T. Wang, G.-M. Tang, W.-Y. Ma, W.-Z. Wan, Polyhedron 26 (2007) 782.
[53] Y.-T. Wang, G.-M. Tang, Z.-W. Qiang, Polyhedron 26 (2007) 4542.
[54] J.P. Jasinski, M.K. Bharty, N.K. Singh, S.K. Kushwaha, R.J. Butcher, J. Chem. Crystallogr. 41 (2011) 6.
[55] T. Akhtar, M.K. Rauf, S. Hameeda, X. Lu, Acta Crystallogr., Sect. E 65 (2009) o2075.
[56] Y.-G. Yan, G.-G. Tu, L.-D. Wang, J. Liu, S.-H. Li, Acta Crystallogr., Sect. E 66 (2010) o1381.
[57] J. Bernstein, R.E. Davies, L. Shimoni, N.L. Chang, Angew. Chem. Int. Ed. Engl. 34 (1995) 1555.
[58] P.M. Anbarasan, M.K. Subramanian, P. Senthilkumar, C. Mohanasundaram, V. Ilangovan, N. Sundaraganesan, J. Chem. Pharm. Res. 3 (2011) 597.
[59] L.J. Bellamy, The Infrared Spectra of Complex Molecules, vol. 2, Chapman and Hall, London, 1980.
[60] R.M. Silverstein, F.X. Webster, D.J. Kiemle, Spectrometric Identification of Organic Compounds, seventh ed., John Willey & Sons, New York, 2005.